Comparative Study of the Effects of Microsilica and Nanosilica in Concrete

Paramita Mondal, Surendra P. Shah, Laurence D. Marks, and Juan J. Gaitero

It is well recognized that the use of mineral admixtures such as silica fume enhances the strength and durability of concrete. This research compares the effects of adding silica fume and nanosilica to concrete and provides a better understanding of the changes in the concrete nanostructure. Nanoindentation with scanning probe microscopy imaging was used to measure the local mechanical properties of cement pastes with 0% and 15% replacement of cement with silica fume. A reduction in the volume fraction of calcium hydroxide in a sample with silica fume provides evidence of pozzolanic reaction. Furthermore, replacing 15% cement by silica fume increased the volume fraction of the high-stiffness calcium silicate hydrate (C-S-H) by a small percentage that was comparable with the decrease in the volume fraction of calcium hydroxide. A parallel study of cement pastes with nanosilica showed that nanosilica significantly improves durability of concrete. This research provides insight into the effects of nanosilica on cement paste nanostructure and explains its effect on durability of concrete. The nanoindentation study showed that the volume fraction of the high-stiffness C-S-H gel increased significantly with addition of nanosilica. Nanoindentation results of cement paste samples with similar percentages of silica fume and nanosilica were compared. Samples with nanosilica had almost twice the amount of high-stiffness C-S-H as the samples with silica fume.

Concrete is a porous material with pore sizes ranging from a few nanometers to a few millimeters. These pores are generally filled with a basic ($pH > 12.5$) pore solution of calcium dissolved in water. Therefore, environmental conditions with lower pH disturb equilibrium and are detrimental to concrete. During the degradation process, known as calcium leaching, caused by exposure to lower pH, cement hydrates progressively dissolve to reestablish the equilibrium concentration of the minerals contained in the pore solution. The dissolution rates of hydration products depend on the calcium-to-silicon ratio of the products, and rates are different for each of the hydrates. Furthermore, the response of each of the hydration products to the attack is also different. Although the phenomenon of calcium leaching has been widely studied, a suitable method to stop it is still unknown. The use of mineral admixtures such as silica fume (SF) is well recognized to enhance the properties of concrete. Silica induces a pozzolanic reaction that results in a reduction of the amount of calcium hydroxide in concrete, and silica fume reduces porosity and improves durability. Recent studies (*1*) have shown that the addition of silica nanoparticles to cement paste could effectively reduce the degradation rate as well as its negative consequences. The aim of this study was to examine the nanomechanical properties of cement pastes with and without silica fume and nanosilica additions. Nanoindentation has been used successfully by researchers to determine the local mechanical properties of cementitious materials (*2–10*). This paper examines the nanomechanical properties of significant phases of cement paste microstructure and concrete by using a special type of nanoindenter called a Triboindenter.

EXPERIMENTAL DETAILS

Materials Used and Sample Preparation

Cement paste samples were made by using type I portland cement (Lafarge). The chemical composition of the cement is SiO_2, 20.4%; CaO, 65.3%; Al_2O_3, 4.8%; Fe_2O_3, 2.8%; C_3S, 68%; and C_3A, 8%. The Blaine surface area was 365 m^2/kg. The specification of ASTM C305 was followed during the mixing of the cement pastes. Samples were cured under water for 1 month at 25°C. To study the effects of silica fume on the nanomechanical properties of the pastes, Force 1000D silica slurry from W. R. Grace was used. Silica slurry is a predispersed mix of silica fume powder in water with 50% total solid by weight. To prepare the paste samples, 15% of cement by weight was replaced by silica fume. The percentage of water present in the slurry was considered to maintain an effective water-to-binder (cement + silica fume) ratio of 0.5. Samples were cured under water for 1 month at 25°C. Figure 1 shows a scanning electron microscope (SEM) image of polished sample with slurry. The effects of the addition of nanosilica on the local mechanical properties of paste microstructure were studied by using commercially available nanosilica. The details of the L100 nanosilica are as follows: commercial name, Levasil 100/45; particle size, 30 nm; SiO_2 content, 45% by weight; stabilizer, NaO; pH, 10; and physical description, colloid. Sample sets with 6% and 18% by weight of nanosilica were studied. Samples were made and cured at the Center for Nanomaterials Applications in Construction of LABEIN-Tecnalia at Derio, Spain. An example of a SEM image of a polished sample with 18% nanosilica is shown in Figure 2. All samples were polished by following the procedure described elsewhere by the authors (*7*). After polishing, significant numbers of indents (140 to 280) were made on each of the samples. Both specimen surface preparation and nanoindentation tests were performed at the Advanced Cement-Based Materials Center at Northwestern University in Evanston, Illinois.

P. Mondal, University of Illinois at Urbana–Champaign, 2114 Newmark Civil Engineering Laboratory, 205 North Mathews Avenue, Urbana, IL 61801-2352. S. P. Shah, Northwestern University, A134 Technological Institute, 2145 Sheridan Road, Evanston, IL 60208-3109. L. D. Marks, Northwestern University, 2220 Campus Drive, B03, EV3108, Evanston, IL 60208. J. J. Gaitero, Labein-Tecnalia, Parque tecnologico de Bizkaia, Edif. 700, 48160 Derio, Spain. Corresponding author: P. Mondal, pmondal@illinois.edu.
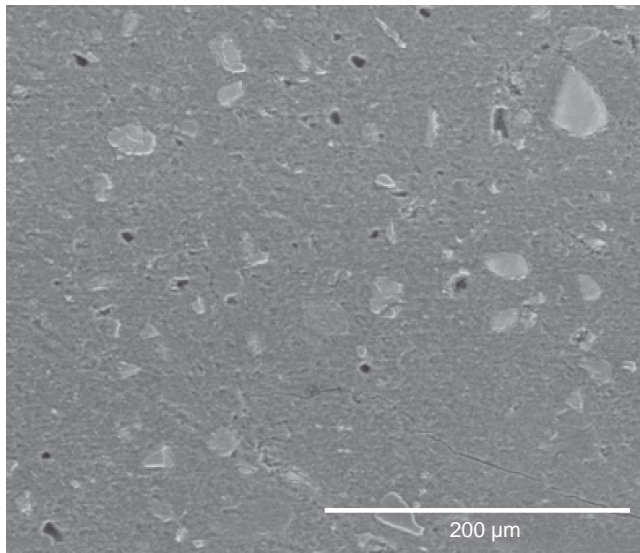
FIGURE 1 Paste with 15% silica fume slurry: SEM image of 1-month-old polished sample.

Nanoindentation Experiments and Data Analysis

A Hysitron Triboindenter was used in this research (Figure 3). A Berkovich tip with a total included angle of 142.3° was used for indentation. Multiple cycles of partial loading and unloading were used to make each indent, thereby eliminating creep and size effects (9). Time to reach maximum load in the first cycle was 10 s, and the loading rate was kept constant for each cycle. Time for complete unload in the last cycle was also 10 s. In each cycle, maximum load was held constant for a period of 5 s. Maximum loads of 750 N were used at a loading rate of 200 N/s. Depth of indentation was within 150 to 250 nm. Some of the indentation test data were discarded due to the irregular nature of the load–displacement plot, which could be due to the presence of large voids at the indentation site or cracking of the material during indentation. The Oliver and Pharr
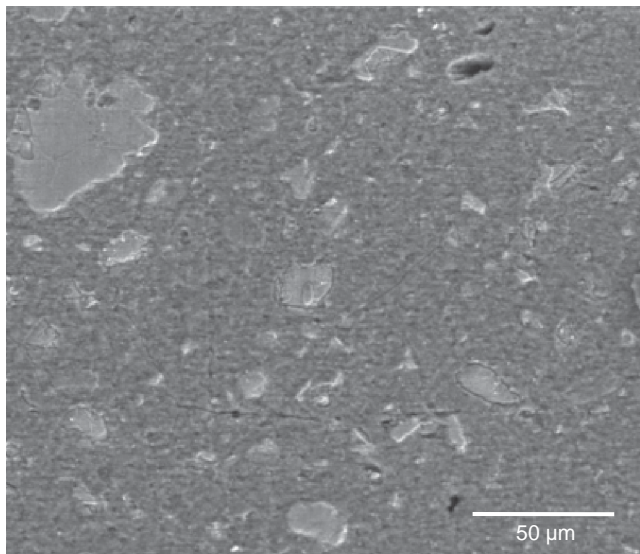

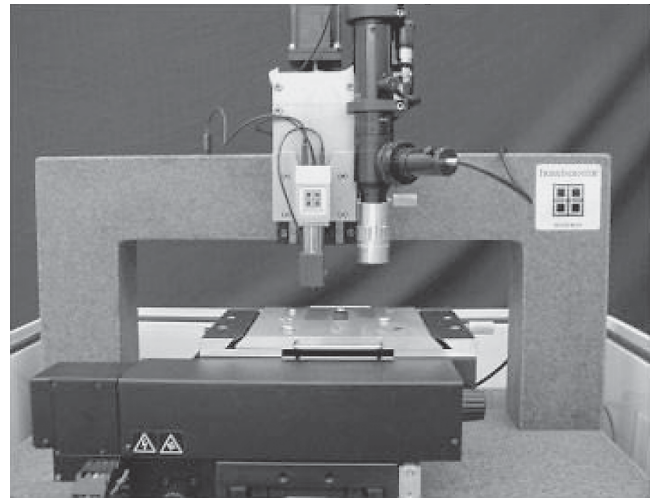FIGURE 2 Paste with 18% nanosilica: SEM image of 1-month-old polished sample.

FIGURE 3 Hysitron Triboindenter.

method (11) was used to evaluate elastic properties by using the final unloading region of the load versus indentation curve (Figure 4). Indentation moduli were calculated from each indent, which is related to the elastic modulus and Poisson's ratio of the particular phase. Because the Poisson's ratios of different phases present in cement paste microstructure were not measured in this study, indentation results were represented in terms of indentation modulus instead of Young's modulus. This is in agreement with recent literature. Furthermore, using an assumed value of the same Poisson's ratio for all phases will change the modulus by the same percentage. This will not affect any conclusions based on comparison of indentation results for different samples.

Grid indentation was performed to determine the volume fractions of different phases present in a sample. On each sample, three different areas were randomly chosen to minimize site-specific properties on the indentation data set. On each area, 144 indents were made in an array in which 12 indents were made in each of 12 rows. Spacing between each indent was 10 µm. An image of the whole area was captured to compare with the modulus map gener-
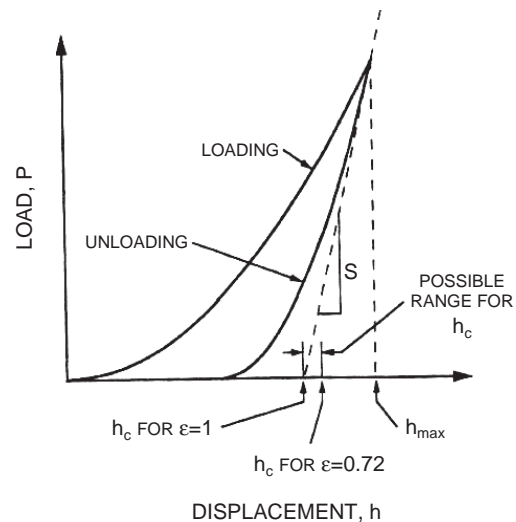

FIGURE 4 Typical load–displacement plot recorded during indentation.

ated from the indentation data. Large volumes of data were analyzed statistically to determine the phase properties and volume fractions of different phases in the paste microstructure. A nonlinear optimization problem was used to fit four normal distributions representing four phases: porous phase, low- and high-stiffness calcium silicate hydrate (C-S-H), and calcium hydroxide. The peak analyzing protocol of commercially available software (Origin) was used to decompose the overall probability distribution obtained into individual probability distributions for each phase. The area under each fitted normal distribution represented the volume fraction of the associated phase.

NANOMECHANICAL PROPERTIES OF MICROSILICA- AND NANOSILICA-MODIFIED CEMENT PASTE

Paste with Silica Fume

Figure 5 shows a 60- × 60-μm image of cement paste with a water-to-cement ratio (w/c) of 0.5 and 0% silica fume. On the image, indentation modulus values are written on their respective indent locations to create a mechanical property map. The elastic modulus of the C-S-H phase was found to be within a range of 10 to 30 GPa, and hardness values ranged from 0.25 to 1 GPa. This matches well with modulus and hardness results reported by other researchers (2–10).

The probability distribution plots of indentation modulus (Figure 6a) and hardness (Figure 6b) are compared for cement paste samples with 0% and 15% silica fume. The bin sizes for the distributions were set at 2.5 GPa and 125 MPa for the elastic modulus and hardness, respectively. Reducing them further would result in excessively irregular distributions due to a limited number of data available in each bin, while further increases would result in a loss of detail. Indentation data were analyzed in terms of their frequency distributions. As C-S-H and other phases present in a cement sample are expected to have a unique set of modulus and hardness, both the
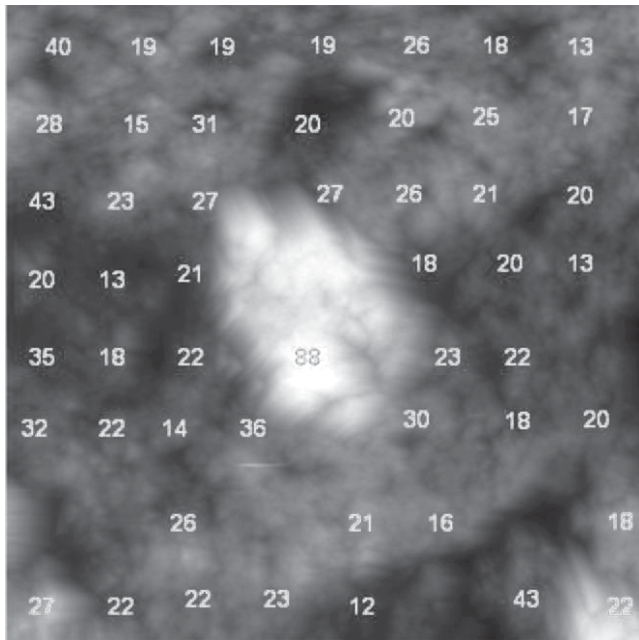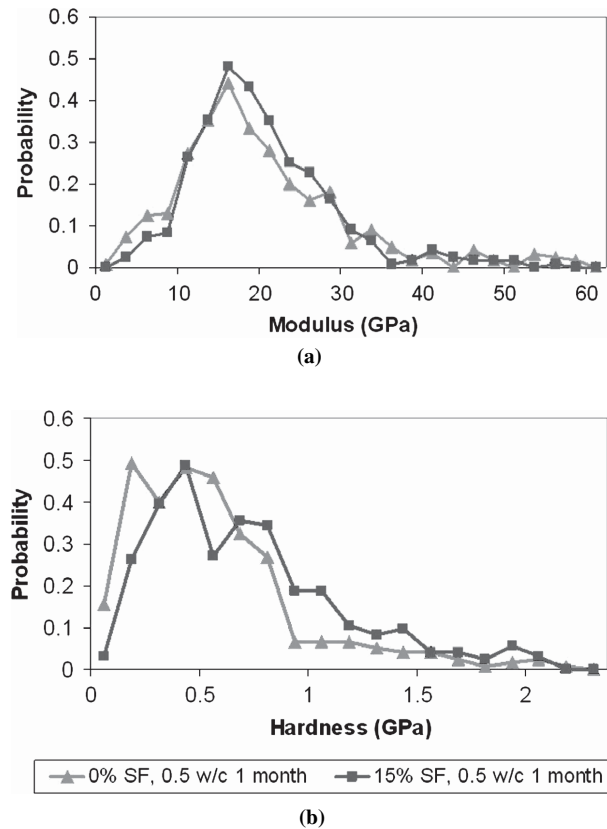

(a)

(b)

FIGURE 6   Probability distributions for (a) modulus and (b) hardness for pastes with 0% and 15% silica slurry.

distributions show a similar trend. In most of the data the modulus ranged between 10 to 30 GPa, and hardness values ranged from 0.25 to 1 GPa, which corresponds to the main phase in cement paste, C-S-H. Furthermore, both modulus and hardness plots show a peak corresponding to calcium hydroxide at a modulus around 33 GPa and hardness around 1.5 GPa. The probability plots shown in Figure 6 were analyzed to determine the volume fraction of C-S-H. Table 1 compares the volume fractions of different phases in samples with 0% and 15% silica fume. The volume fraction of the porous phase was comparable in samples with and without silica fume. However,

FIGURE 5   60- × 60-μm image of cement paste with 0.5 w/c showing indentations and modulus (in GPa) written on each indent location.

TABLE 1   Change in Volume Fraction of Different Phases in Cement Paste with Addition of 0% and 15% Silica Fume

	Silica Fume	
	0%	15%
Porous phase		
Elastic modulus (GPa)	9.4 ± 3.4	10 ± 4.2
Volume fraction (%)	10	12
Low stiffness C-S-H		
Elastic modulus (GPa)	16.5 ± 4.7	17.5 ± 3.7
Volume fraction (%)	63	60
High stiffness C-S-H		
Elastic modulus (GPa)	27.1 ± 3.5	26.0 ± 3.4
Volume fraction (%)	19	25
Calcium hydroxide		
Elastic modulus (GPa)	36.9 ± 3.5	31.8 ± 3.4
Volume fraction (%)	8	3

nanoindentation results showed evidence of pozzolanic reaction in the sample with silica fume. Table 1 clearly shows that the addition of silica fume increased the volume fraction of high-stiffness C-S-H and decreased the volume fraction of calcium hydroxide. This observation is particularly interesting since it compares well with literature reporting an increase in the volume fraction of C-S-H with longer chain length in blended cement paste with silica fume (*12*).

Paste with Nanosilica

Since it is known that ^{29}Si magic angle spinning–nuclear magnetic resonance (MAS-NMR) spectra of cement pastes with nanosilica show that nanoparticles increase the average chain length of C-S-H gel, it was expected that nanosilica either increased the amount or the strength of high-stiffness C-S-H (*1*). Grid indentation data were analyzed in terms of their frequency distributions. Table 2 contains the results obtained from the study of two pastes containing 6% and 18% by weight of colloidal nanosilica. Table 2 confirms that nanosilica does not change the average values of the hardness and modulus of any of the phases of C-S-H gel. On the contrary, it modifies the relative proportions of the two C-S-H phases, promoting formation of the high-stiffness phase over the low-stiffness one. Volume fractions of high-stiffness C-S-H were 38% and 50% for samples with 6% and 18% nanosilica, respectively. This has significance on durability of concrete. Gaitero et al. (*1*) reported that high-stiffness C-S-H is more resistant to calcium leaching. Therefore, addition of nanosilica has a positive impact on durability.

CONCLUSIONS

1. From nanoindentation experiments, unhydrated cement particles were found to have an elastic modulus around 100 GPa, which is much higher than their products of hydration. The elastic modulus of unhydrated cement particles found in this study is little lower than the results reported by Velez et al. (*10*), which are attributed to the porosity within cement particles.

2. The elastic modulus of the C-S-H phase was found to be within a range of 10 to 30 GPa, and hardness values ranged from 0.25 to 1 GPa. These values match well with modulus and hardness results reported by other researchers (*2–10*).

3. Replacing 15% cement by silica fume did not change the elastic moduli of the four phases. A reduction in the volume fraction of calcium hydroxide in the sample with silica fume provides evidence of pozzolanic reaction. An increase in the volume fraction of high-stiffness C-S-H was observed that was comparable with the decrease in the volume fraction of calcium hydroxide. This hints

that either pozzolanic reaction forms more high-stiffness C-S-H or improved packing in a sample with silica fume facilitates formation of high-stiffness C-S-H and thus increases the ratio of high-stiffness to low-stiffness C-S-H by 10%. Further study of changes in the morphology of C-S-H due to addition of silica fume is needed to explore these possibilities.

4. In a study done parallel to this research, ^{29}Si MAS-NMR spectra of the cement pastes with nanosilica proved that nanosilica increases the average chain length of C-S-H gel. Therefore, it was expected that nanosilica increases either the amount of high-stiffness C-S-H or its strength. Nanoindentation studies proved that neither of the elastic moduli of the two C-S-H phases changed with the addition of nanosilica. However, nanosilica increased the amount of high-stiffness C-S-H gel significantly. In samples with 18% nanosilica, the volume fraction of high-stiffness C-S-H was as high as 50%. This explains the positive impact on durability of adding nanosilica to concrete, as Gaitero et al. (*1*) report that high-stiffness C-S-H is more resistant to calcium leaching.

REFERENCES

1. Gaitero, J. J., I. Campillo, and A. Guerrero. Reduction of the Calcium Leaching Rate of Cement Paste by Addition of Silica Nanoparticles. *Cement and Concrete Research,* Vol. 38, 2008, pp. 1112–1118.
2. Constantinides, G., and F.-J. Ulm. The Effect of Two Types of C-S-H on the Elasticity of Cement-Based Materials: Results from Nanoindentation and Micromechanical Modeling. *Cement and Concrete Research,* Vol. 34, 2004, pp. 67–80.
3. Constantinides, G., F.-J. Ulm, and K. van Vliet. On the Use of Nanoindentation for Cementitious Materials. *Materials and Structures/ Matériaux et Constructions,* Vol. 36, No. 257, 2003, pp. 191–196.
4. Constantinides, G., and F.-J. Ulm. The Nanogranular Nature of C-S-H. *Journal of the Mechanics and Physics of Solids,* Vol. 55, No. 1, 2007, pp. 64–90.
5. Hughes, J. J., and P. Trtik. Micro-Mechanical Properties of Cement Paste Measured by Depth-Sensing Nanoindentation: A Preliminary Correlation of Physical Properties with Phase Type. *Materials Characterization,* Vol. 53, No. 2–4, 2004, pp. 223–231.
6. Mondal, P., S. P. Shah, and L. D. Marks. A Reliable Technique to Determine the Local Mechanical Properties at the Nano-Scale for Cementitious Materials. *Cement and Concrete Research,* Vol. 37, 2007, pp. 1440–1444.
7. Mondal, P., S. P. Shah, and L. D. Marks. Nano-Scale Characterization of Cementitious Materials. *ACI Materials Journal,* Vol. 105, No. 2, 2008, pp. 174–179.
8. Mondal, P., S. P. Shah, and L. D. Marks. Use of Atomic Force Microscopy and Nanoindentation for Characterization of Cementitious Materials at the Nanoscale. In *SP-254: Nanotechnology of Concrete: Recent Developments and Future Perspectives,* American Concrete Institute, Farmington Hills, Mich., 2008.
9. Němeček, J., L. Kopecký, and Z. Bittnar. Size Effect in Nanoindentation of Cement Paste. In *Application of Nanotechnology in Concrete Design* (R. K. Dhir, M. D. Newlands, and L. J. Csetenyi, eds.), Thomas Telford, London, 2005, pp. 47–53.
10. Velez, K., S. Maximilien, D. Damidot, G. Fantozzi, and F. Sorrentino. Determination by Nanoindentation of Elastic Modulus and Hardness of Pure Constituents of Portland Cement Clinker. *Cement and Concrete Research,* Vol. 31, 2001, pp. 555–561.
11. Oliver, W. C., and G. M. Pharr. An Improved Technique for Determining Hardness and Elastic Modulus Using Load and Displacement Sensing Indentation Experiments. *Journal of Materials Research,* Vol. 7, 1992, pp. 1564–1583.
12. Richardson, I. G. Tobermorite/Jennite– and Tobermorite/Calcium Hydroxide–Based Models for the Structure of C-S-H: Applicability to Hardened Pastes of Tricalcium Silicate, β-Dicalcium Silicate, Portland Cement, and Blends of Portland Cement with Blast-Furnace Slag, Metakaolin, or Silica Fume. *Cement and Concrete Research,* Vol. 34, 2004, pp. 1733–1777.

TABLE 2   Change in Volume Fraction of Different Phases in Cement Paste with Addition of 6% and 18% by Weight of Nanosilica

	Nanosilica	
	6 wt%	18 wt%
Low stiffness C-S-H		
Elastic modulus (GPa)	17.0 ± 1.0	18.9 ± 0.4
Volume fraction (%)	44	37
High stiffness C-S-H		
Elastic modulus (GPa)	23.7 ± 0.7	26.7 ± 0.8
Volume fraction (%)	38	50